IV International Conference on Computational Methods for Coupled Problems in Science and Engineering
COUPLED PROBLEMS 2011
M. Papadrakakis, E. Oñate and B. Schrefler (Eds)

MULTI-SCALE ANALYSIS ON CAVITATION DAMAGE AND ITS MITIGATION FOR THE SPALLATION NEUTRON SOURCE

KOHEI OKITA*, KENJI ONO*, SHU TAKAGI† AND YOICHIRO MATSUMOTO†

* Functionality Simulation and Information Team, VCAD System Research Program, RIKEN
Hirosawa 2-1, Wako-shi, Saitama, 351-0198, Japan
e-mail: {okita, keno}@riken.jp, www.riken.go.jp

† Department of Mechanical Engineering, the University of Tokyo
Hongo 7-3-1, Bunkyo-ku, Tokyo, 113-8656, Japan
e-mail: {takagi, ymats}@mech.t.u-tokyo.ac.jp, www.u-tokyo.ac.jp

Key words: Pressure Wave Propagation, Bubbly Flows, Spallation Neutron Source, Cavitation Erosion, Fluid Structure Interaction

Abstract. *Impact of injecting microbubbles on the thermal expansion due to the nuclear spallation reaction were examined numerically. Since the mercury density is higher than the density of solid wall, the interaction between mercury and solid wall must be taken into account. Our approach is to solve the momentum and energy conservation equations and the time development of elastic stress for both bubbly fluid and elastic solid. The Keller equation is employed to reproduce the nonlinear oscillation of bubble with considering the thermal dumping effect by the reduced order model. The continuum phase of liquid mercury is coupled with the discrete phase of microbubbles using the Euler-Lagrange method. As the results, the bubble cloud develops around the center of inertia of motion induced by the thermal expansion. The elasticity of the wall affects on the migration of the center of inertia away from the wall. The injection of microbubbles is effective to decrease the pressure rise due to thermal expansion for both rigid and elastic wall conditions when the void fraction of microbubbles is higher than the volume rate of thermal expansion of liquid mercury.*

1 INTRODUCTION

Japan proton accelerator research complex (J-PARC) was constructed as a spallation neutron source in Japan. The heat generation of the nuclear spallation reaction causes the thermal expansion of liquid mercury, which produces high pressure waves. When the pressure waves hit a casing wall, cavitation occurs and erodes the wall [1]. To mitigate the cavitation erosion, a method of introducing gas bubbles into liquid mercury has been proposed [2]. The method has expected that the microbubbles absorb the thermal expansion of liquid mercury and attenuate the pressure waves.

The propagation of pressure waves caused by a thermal shock in liquid mercury containing microbubbles has been numerically investigated in the previous work [3]. The influences of the injecting bubble size and void fraction on the absorption of the thermal expansion of liquid mercury and the attenuation of pressure waves have clarified as follows. Firstly, if the void fraction is higher than the volume rate of thermal expansion of liquid mercury, the

pressure rise due to thermal expansion decreases with decreasing bubble radius, because of the increase of the natural frequency of bubble in bubbly mixture. Secondly, as the bubble radius increases, the peak of pressure waves which propagate at the sound speed of mixture decreases due to the dispersion effect of bubbly mixture. In the case of liquid mercury containing large bubbles whose natural frequency is lower than the frequency of thermal shock, the pressure waves propagates at the sound speed of the liquid mercury and increases the peak pressure at the wall. Thirdly, the comparison with and without heat transfer through the gas liquid interface shows that the pressure waves are attenuated by the thermal damping effect even if the decrease of the void fraction makes the behaviour of bubbles nonlinear.

Since the density of liquid mercury (13,579kg/m^3) is higher than the density of solid wall (316SS, 7,946kg/m^3), the impact of the interaction between liquid mercury and wall on cavitation erosion should be considered when the pressure waves hit the wall. Therefore, we extend the previous work to consider the elasticity of wall in a two-dimensional computation.

Our approach is to solve the mass, momentum and energy conservation equations for bubbly fluid with the equation of state of liquid mercury to reproduce the pressure rise due to thermal shock. The Euler-Lagrange method is used for coupling the liquid mercury and microbubbles. The nonlinear oscillation of bubble dynamics is described by the Keller equation with an assumption of spherical bubble. The thermal dumping effect due to the heat transfer through the bubble interface is taken into account using the reduced order model. The elastic wall is represented by solving the equations for elastic body.

In the present paper, firstly, basic equations are introduced to reproduce the propagation of pressure waves caused by a thermal shock in liquid mercury containing microbubbles with taking into account the interaction between bubbly fluids and elastic wall. Secondly, the numerical method and model are mentioned. Finally, the impacts of the interaction of the thermal expansion of liquid mercury and the wall on the pressure rise due to thermal expansion and the distribution of bubble clouds are discussed.

2 BASIC EQUATIONS

2.1 Discrete phase of bubbles

To describe the dynamics of spherical bubble of radius R, the Keller equation [4][5] is employed

$$\begin{aligned}&\left[1-\frac{1}{c_s}\frac{dR}{dt}\right]R\frac{d^2R}{dt^2}+\frac{3}{2}\left[1-\frac{1}{3c_s}\frac{dR}{dt}\right]\left(\frac{dR}{dt}\right)^2\\&=\frac{1}{\rho}\left[1+\frac{1}{c_s}\frac{dR}{dt}+\frac{1}{c_s}R\frac{d}{dt}\right]\left(P_G-\frac{2\sigma}{R}-\frac{4\mu}{R}\frac{dR}{dt}-P_L\right)\end{aligned} \tag{1}$$

where c_s is the sound speed of surrounding liquid, ρ is liquid density, σ is surface tension and μ is liquid viscosity. If the bubble boundary moves with a velocity much lower than the speed of sound in the gas, the pressure of gas inside bubble P_G can be taken as uniform and is expressed as

$$\frac{dP_G}{dt} = -3\gamma P_G \frac{1}{R}\frac{dR}{dt} + \frac{3(\gamma-1)}{R} K \left.\frac{\partial T}{\partial r}\right|_{r=R}, \tag{2}$$

where γ is the ratio of specific heats [6]. The second term on the right hand side represents the heat transfer between the gas inside bubble and the surrounding liquid. The temperature gradient at the bubble boundary is estimated by a reduced order model [7] instead of directly solving the energy equation for the temperature distribution inside bubble. The reduced order model is briefly described as follows.

The temperature gradient at the bubble boundary is modeled as

$$\left.\frac{\partial T}{\partial r}\right|_{r=R} = \frac{\mathrm{Re}\left(\tilde{L}_P\right)}{\left|\tilde{L}_P\right|^2}\left(T_0 - T_b\right) + \frac{\mathrm{Im}\left(\tilde{L}_P\right)}{\left|\tilde{L}_P\right|^2}\frac{1}{\omega_N}\frac{dT_b}{dt}, \tag{3}$$

where $T_b = P_G R^3 T_b / P_{G0} R_0^3$ is the representative temperature of the gas inside bubble. The natural frequency of bubble ω_N is described by

$$\omega_N^2 = \frac{\mathrm{Re}\left(\Upsilon_N\right) P_G}{\rho R^2}\frac{T_0}{T_b} - \frac{2\sigma}{\rho R^3} - \frac{4}{\rho^2 R^4}\left[\mu + \frac{\mathrm{Im}\left(\Upsilon_N\right) P_G}{4\omega_N}\frac{T_0}{T_b}\right]^2 \tag{4}$$

where Υ_N is a complex function defined by

$$\Upsilon_N = \frac{3\alpha_N^2\gamma}{\alpha_N^2 + 3(\gamma-1)\left(\alpha_N \coth\alpha_N - 1\right)} \tag{5}$$

with

$$\alpha_N^2 = i\frac{\gamma\omega_N P_G R^2}{(\gamma-1)T_b K_0}. \tag{6}$$

The thermal penetration length $\tilde{L}_P$ is also a complex function and is described as

$$\tilde{L}_P = \frac{\alpha_N^2 - 3\left(\alpha_N \coth\alpha_N - 1\right)}{\alpha_N^2\left(\alpha_N \coth\alpha_N - 1\right)} R \tag{7}$$

The temperature gradient at a boundary can be obtained by solving equations (3) to (7). Then the pressure inside is updated according to Eq.(2).

In the present study, bubbles are treated in a Lagrangian way. Due to the assumption of the no-slip condition, the bubble velocity is the same as the bubbly mixture velocity. The position of the each bubble is then traced by

$$\mathbf{x}_B = \int \mathbf{u}\left(\mathbf{x}_B\right) dt. \tag{8}$$

2.2 Continuum phase of bubbly fluid and elastic solid

Since the acoustic Mach number is low, the advection term assumes to be negligible. Then, the momentum equation can be represented

$$\rho \frac{\partial \mathbf{v}}{\partial t} = \nabla \cdot \boldsymbol{\sigma} . \tag{9}$$

The total strain rate is

$$\mathbf{e} = \frac{1}{2}\left\{ \nabla \mathbf{v} + \left(\nabla \mathbf{v} \right)^T \right\}, \tag{10}$$

and includes the elastic strain rate, thermal strain rate and the volumetric strain rate due to bubble oscillation as $\mathbf{e} = \mathbf{e}_E + \mathbf{e}_T + \mathbf{e}_B$. Assuming the small strain, Hook's low for isotropic linear elasticity is employed for the elastic strain. The time development of elastic stress can be described

$$\frac{\partial \boldsymbol{\sigma}}{\partial t} = -\frac{\partial p}{\partial t}\mathbf{I} + 2\mu \left(\mathbf{e} - \frac{1}{3}\mathrm{tr}\left(\mathbf{e} \right)\mathbf{I} \right), \tag{11}$$

where μ is shear modulus. The time development of pressure is defined by

$$\frac{\partial p}{\partial t} = -\zeta \left[\mathrm{tr}\left(\mathbf{e} \right) - \mathrm{tr}\left(\mathbf{e}_B \right) - \mathrm{tr}\left(\mathbf{e}_T \right) \right] \tag{12}$$

where ζ is bulk modulus. The volume change due to bubble oscillation is described using the void fraction of bubbles f_G [8]

$$\mathrm{tr}\left(\mathbf{e}_B \right) = \frac{1}{1 - f_G}\frac{\partial f_G}{\partial t} . \tag{13}$$

And the thermal volumetric strain rate can be described using the thermal expansion rate at constant pressure $\beta = \left(1/V \right)\left(\partial V / \partial T \right)_p$ [9] as

$$\mathrm{tr}\left(\mathbf{e}_T \right) = \frac{\beta}{C_p} T \frac{\partial S}{\partial t} . \tag{14}$$

Both a temperature diffusion and the heat generation due to the nuclear spallation reaction are taken into account in the energy equation

$$\rho T \frac{\partial S}{\partial t} = \nabla \cdot \left(k \nabla T \right) + Q . \tag{15}$$

Substituting Eq.(15) to Eq.(14), the thermal volumetric strain rate becomes

$$tr\left(\mathbf{e}_T \right) = \frac{\beta}{\rho C_p}\left[\nabla \cdot \left(k \nabla T \right) + Q \right]. \tag{16}$$

On the other hand, using the thermodynamic relation as $TdS = C_p dT - \left(\beta T / \rho \right) dp$ [9], the time development of temperature can be described

$$\rho C_p \frac{\partial T}{\partial t} = \beta T \frac{\partial p}{\partial t} + \nabla \cdot \left(k \nabla T \right) + Q . \tag{17}$$

In the present study, two volume fractions are introduced. Firstly, the volume fraction of solid phase is employed to distinguish solid phase from fluid phase. Secondly, the volume fraction of gas is defined as the volume ratio of bubble in the fluid phase. The mixture density of fluids and solid is described as $\rho = (1-\phi_S)\rho_F + \phi_S\rho_S$, where the density of fluid phase can be assumed as $\rho_F = (1-f_G)\rho_L$ because of low density and low void fraction of gas. Then the mixture density becomes

$$\rho = (1-\phi_S)(1-f_G)\rho_L + \phi_S\rho_S . \tag{18}$$

Specific heat and thermal expansion rate at constant pressure are represented respectively,

$$\rho C_p = (1-\phi_S)(1-f_G)\rho_L C_{pL} + \phi_S\rho_S C_{pS} \tag{19}$$

and

$$\beta = (1-\phi_S)(1-f_G)\beta_L + \phi_S\beta_S . \tag{20}$$

The coefficients, bulk modulus, shear modulus and thermal conductivity are calculated by the harmonic average using the volume fraction of solid phase as

$$\frac{1}{\zeta} = \frac{1-\phi_S}{\zeta_L} + \frac{\phi_S}{\zeta_S} . \tag{21}$$

The density and bulk modulus of liquid phase is obtained from pressure and temperature through the equation of state for liquid mercury [3].

3 NUMERICAL METHODS

The basic equations are solved using a second-order finite difference scheme based on the FDTD method [10]. To resolve the rebound of bubble collapse, the Keller equation is integrated in adaptive time increments, which are always smaller than the time increment for the integration of the basic equations for the mixture. Bubbles are described by the representative bubble at the Lagrange point and coupled with mixture phase by the Euler-Lagrange method, which requires the interpolation of physical values between Euler and Lagrange points. The void fraction at the Euler point is obtained by

$$f_G(\mathbf{x}) = \int f_G(\mathbf{x}')\delta_\varepsilon(\mathbf{x}'-\mathbf{x})d\mathbf{x}' = \sum_k \frac{\frac{4}{3}\pi n_{Bk}R_k^3}{V_k} D_\varepsilon(\mathbf{x}_{Bk}-\mathbf{x}) \tag{22}$$

where n_B is the number weight of the representative bubble and D_ε is defined by

$$D_\varepsilon(\mathbf{x}) = \begin{cases} \prod_{i=1}^{2}\left[\frac{\Delta x_i}{2\varepsilon}\left\{1+\cos\left(\frac{\pi x_i}{\varepsilon}\right)\right\}\right], & for\ |x_i| \le \varepsilon \\ 0, & othre\ wise \end{cases} . \tag{23}$$

The width of the smooth delta function ε is taken as Δx. On the other hand, the pressure and velocity of the mixture at the bubble position, which are required to solve Eq. (1) and Eq. (8), are interpolated, respectively, as follows:

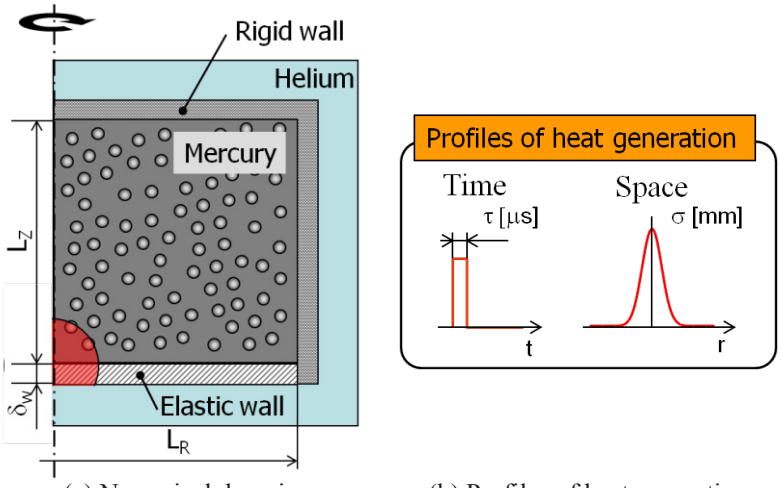

(a) Numerical domain (b) Profiles of heat generation

Figure 1: Schematic diagram of the numerical model. The bubbly liquid mercury is surrounded by the rigid and elastic wall of the cylinder, in which helium microbubbles uniformly distribute. The heat generation is introduced at the center bottom.

$$P_L(\mathbf{x}_B) = \sum_{\mathbf{x}} p(\mathbf{x}) D_\varepsilon(\mathbf{x} - \mathbf{x}_B) \text{ and } \mathbf{u}(\mathbf{x}_B) = \sum_{\mathbf{x}} \mathbf{u}(\mathbf{x}) D_\varepsilon(\mathbf{x} - \mathbf{x}_B). \quad (24)$$

4 NUMERICAL MODEL

Bubbly liquid mercury in a cylinder is considered as shown in Fig.1(a). Helium microbubbles uniformly distribute in the liquid mercury. The sizes of numerical domain are L_R=30mm and L_Z=30mm, which is resolved by 200 × 200 grid points. The width of bottom wall is δ_W=1.5mm resolved by 10 grid points. The properties of the solid material of 316SS are density ρ_S=7,964kg/m^3, Young's modulus E_S=195GPa and Poisson ratio ν_S=0.27. A heat generation is introduced around the center bottom of the cylinder to represent a spallation neutron reaction. The profiles of the heat generation are 1μs rectangular pulse in time and Gaussian distribution of the standard deviation σ=5mm in space as shown in Fig.1(b). That induces the thermal expansion of liquid mercury and pressure rises. Pressure waves then propagate through the bubbly liquid mercury. We chose the maximum of the heat generation as $Q_{\max}$=26.7×10^{12}W/m^3 to reproduce the pressure rise of the order of tens MPa in the case without microbubbles.

5 RESULTS

Influences of the elasticity of the bottom wall are examined without microbubbles. The time evolution of the pressure distribution for the elastic wall is compared with that for the rigid wall in Fig.2. In the case of the elastic wall, the pressure around the center bottom changes as plus, minus and plus in time. The pressure propagates upward unlike with the spherical pressure propagation of the rigid wall. The profiles of the pressure at points of z=0, 4.5mm on the axis of the cylinder are shown in Fig.3 with comparing for the rigid and elastic wall conditions. The elasticity of the solid wall decreases the pressure fluctuation induced by the thermal expansion at z=0mm as shown in Fig.3(a). However, as shown in Fig.3(b), the

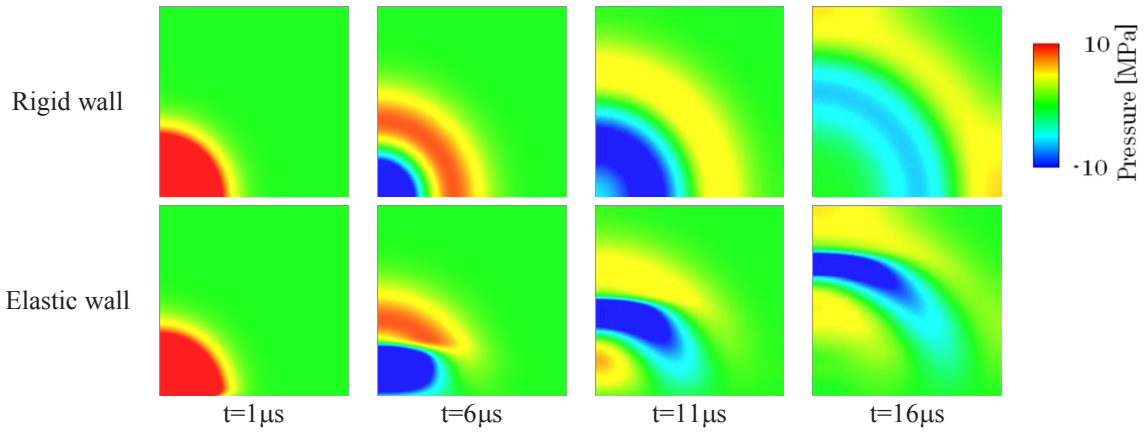

Figure 2: Influence of elastisity of bottom wall on the development of pressure distribution without microbubbles.

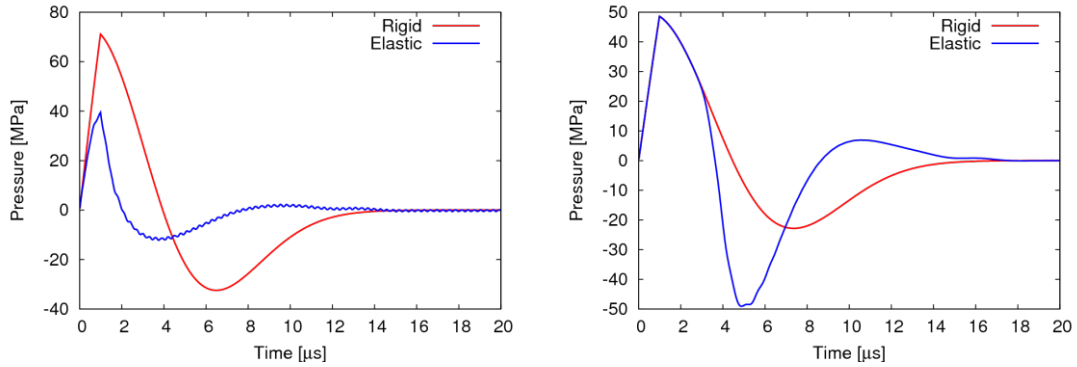

(a) z=0mm (b) z=4.5mm

Figure 3: Influence of elastisity of bottom wall on the profiles of the pressure at z=0, 4.5mm without microbubbles.

negative pressure becomes lower than that for the rigid wall. This is because the center of inertia of the motion induced by the thermal expansion is moved upward away from the center of heat generation owing to the elasticity of the wall, whose density of the solid wall is lower than the mercury density. Such negative pressure is closely related with the growth of bubble clouds. We have focused on the production of the bubble cloud after the thermal expansion of liquid mercury.

Influences of the elasticity of the bottom wall on the production of the bubble cloud are examined by injecting microbubbles to liquid mercury with bubble diameter d=10μm and initial void fraction f_{G0}=0.05%. Figure 4 shows the time evolution of the pressure and void fraction distributions for the rigid and elastic wall conditions. As shown in Fig.4(a), pressure waves spherically propagate under the rigid wall condition at the slower speed than the sound speed of mercury. The bubble clouds also spherically grow up at the center bottom. On the other hand, the bubble clouds grow up away from the wall in the case of the elastic wall. The shape of the bubble clouds is like a squashed sphere as shown in Fig.4(b). The pressure fluctuations are observed between the bubble clouds and the elastic wall. The profiles of the pressure and void fraction at points of z=0, 4.5mm on the axis of the cylinder are shown in

Fig.5. The pressure increase to around 60MPa for the rigid wall and to around 35MPa for the elastic wall at the point of z=0mm. The peaks of pressure for both conditions are lower than the peaks without microbubbles. This is due to the contraction of the injected microbubbles. As shown in Fig.5(a), the pressure at z=0mm fluctuates in the case of the elastic wall. Negative pressure as shown in Fig.3 is disappeared owing to the microbubbles. The void fraction at z=0mm for the rigid wall is higher than that for the elastic wall. Contrary, the void fraction at z=4.5mm for the rigid wall is lower than that for the elastic wall. This is because the center of inertia of motion induced by the thermal expansion is away from the wall as shown in Fig.4. Thus the bubble cloud develops around the center of inertia of motion induced by the thermal expansion of liquid mercury. The elasticity of the wall impacts on the migration of the center of inertia away from the wall.

Here, the volume rate of thermal expansion of liquid mercury is estimated as

$$\Delta f_L = \frac{\beta_L Q_{\max} \Delta \tau}{\rho_L C_{pL}} . \tag{25}$$

It becomes Δf_L=0.26% for β_L=182×10^{-6}K^{-1}, ρ_L=13,579kg/m^3, C_{pL}=139J/kg·K, $Q_{\max}$=26.7×10^{12}W/m^3 and $\Delta\tau$=1μs. So it is required for the mitigation of the pressure rise that the initial void fraction of microbubbles is higher than the volume rate of thermal expansion of liquid mercury Δf_L=0.26%.

Next, calculations under the condition of the initial void fraction of f_{G0}=0.5% are performed. The diameter of microbubbles is 10μm. Figure 6 shows the time evolution of the pressure and void fraction distribution for the rigid and elastic wall condition. The time evolution of the pressure distribution for both is similar to that without microbubbles as shown in Fig.2. But the time scale with microbubbles is much longer due to the slower sound speed of bubbly liquid. On the other hand, the time evolution of the void fraction distribution well follows the pressure distribution. The void fraction decreases in the high pressure region and decreases in the low pressure region.

Figure 7 shows the profiles of the pressure and void fraction for the rigid and elastic wall conditions. Obviously, the pressure rise decreases in both conditions as shown in Fig.7(a) and (b). The intensity of pressure at z=0mm is around 2.5MPa, which is much lower than that without microbubbles. The fluctuations of pressure at z=0mm and 4.5mm are observed in t=0~4μs. This is due to the bubble oscillation with the natural frequency of bubble in bubbly liquid [3]. For the elastic wall, the pressure at z=0mm continuously fluctuates owing to the oscillation of the elastic wall. As shown in Fig.7(c) and (d), the void fraction at z=0mm decreases from 0.5% to 0.25% in t=0~1μs. The difference of the void fraction is around 0.25%, which approximately corresponds to the volume rate of thermal expansion of liquid mercury Δf_L=0.26%. Thus, the injection of microbubbles is effective to decrease the pressure rise due to thermal expansion of liquid mercury for both rigid and elastic wall conditions when the void fraction of microbubbles is higher than the volume rate of thermal expansion of liquid mercury.

6 CONCLUSIONS

To investigate the cavitation erosion and its mitigation for the nuclear spallation source, the impacts of injecting microbubbles on the thermal expansion due to a nuclear spallation

reaction were examined numerically. The interaction between liquid mercury and solid wall was taken into account by solving the momentum and energy conservation equations and the time development of elastic stress for both fluid and solid phases. Additionally, the nonlinear oscillation of bubbles was reproduced using Keller equation with considering the thermal dumping effect by the reduced order model.

As the result of the calculation, the bubble cloud develops around the center of inertia of motion induced by the thermal expansion of liquid mercury. The elasticity of the wall affects on the migration of the center of inertia away from the wall.

The injection of microbubbles is effective to decrease the pressure rise due to thermal expansion of liquid mercury for both rigid and elastic wall conditions when the void fraction of microbubbles is higher than the volume rate of thermal expansion of liquid mercury.

REFERENCES

[1] Futakawa M., Naoe T., Tsai, C.C., Ishikura S., Ikeda Y., Soyama H., Date H., Cavitation erosion in mercury target of spallation neutron source, *Proceedings of Fifth International Symposium on Cavitation, Osaka, November 1-4* (2003).

[2] Hansen G., Butzek M., Glückler H., Hanslik R., Sotner H., Soukhnov V., Stelzer H., Wolters J., Engineering work for the ESS target station. *Proceedings of the Sixth International Topical Meeting on Nuclear Applications of Accelerator Technology, San Diego, june 1-5*(2003).

[3] Okita K., Takagi S., Matsumoto Y., Propagation of Pressure Waves, Caused by a Thermal Shock, in Liquid Metals Containing Gas Bubbles, *Journal of Fluid Science and Technology*, (2008) **3**(1):116-128.

[4] Keller J.B., Kolodner I.I., Damping of underwater explosion bubble oscillations, *J. Appl. Phys.* (1956) **27**(10):1152-1161.

[5] Prosperetti A., Lezzi A., Bubble dynamics in a compressible liquid. part 1. first-order theory, *J. Fluid Mech* (1986) **168**:457-478.

[6] Prosperetti A., The thermal behavior of oscillating gas bubbles, *J. Fluid Mech.* (1991) **222**:587-616.

[7] Sugiyama K., Takagi S. and Matsumoto Y., A New reduced-Order Model for the Thermal Damping Effect on Radial Motion of a Bubble (2nd Report, Validation of the Model by Numerical Simulation), *Trans. JSME Ser. B* (2004) **71**:1011-1019.

[8] Commander K.W. and Prosperetti A., Linear pressure waves in bubbly liquids: Comparison between theory and experiments, *J. Acoust. Soc. Am.* (1989) **85**(2):732-746.

[9] Batchelor G.K., 1.5 Classical thermodynamics in *An Introduction to Fluid Dynamics*, *Cambridge University Press* (2000).

[10] Yee K.S., Numerical solution of initial boundary value problems involving Maxwell's equations in isotropic media, *IEEE Trans. Antennas Propag.* (1996) **14**(8):301-307.

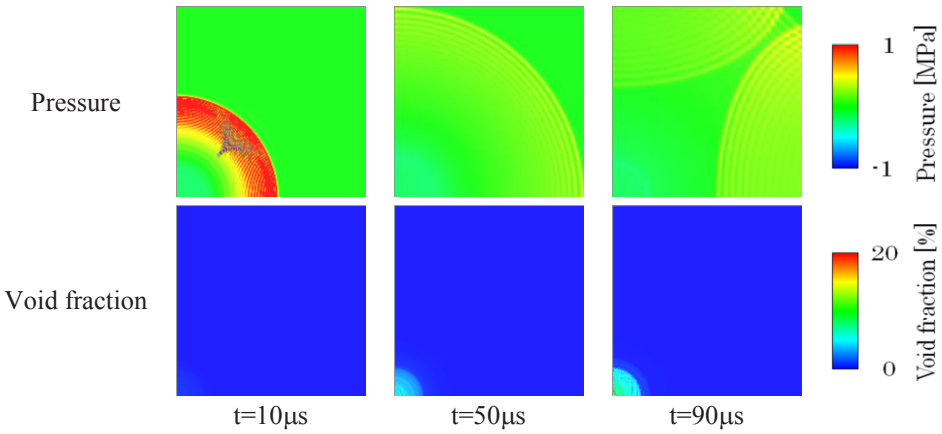

(a) Rigid wall

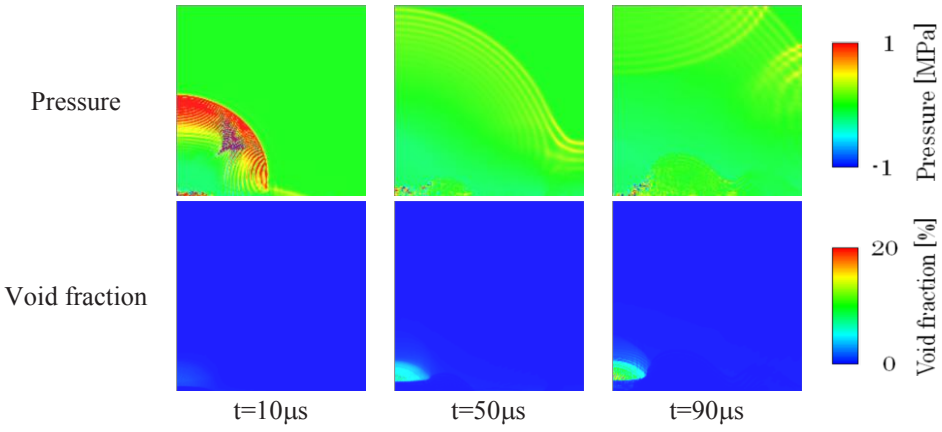

(b) Elastic wall

Figure 4: Time evolution of the pressure and void fraction distribution for f_{G0}=0.05%.

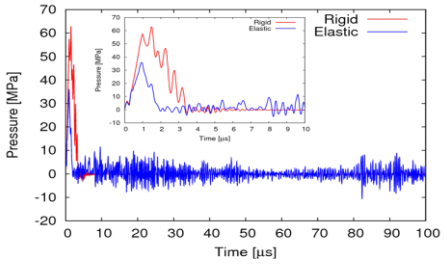

(a) Pressure at z=0mm

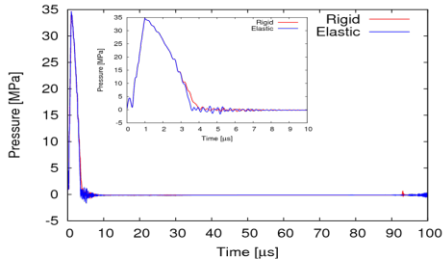

(b) Pressure at z=4.5mm

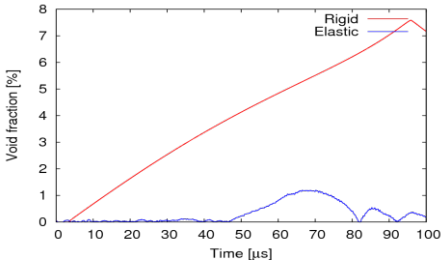

(c) Void fraction at z=0mm

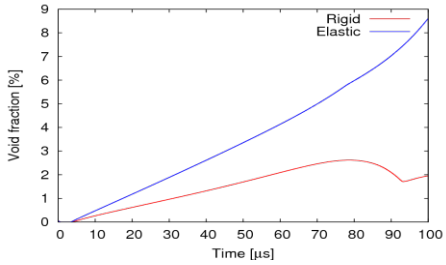

(d) Void fraction at z=4.5mm

Figure 5: Profile of the pressure and void fraction at points of z=0, 4.5mm for f_{G0}=0.05%.

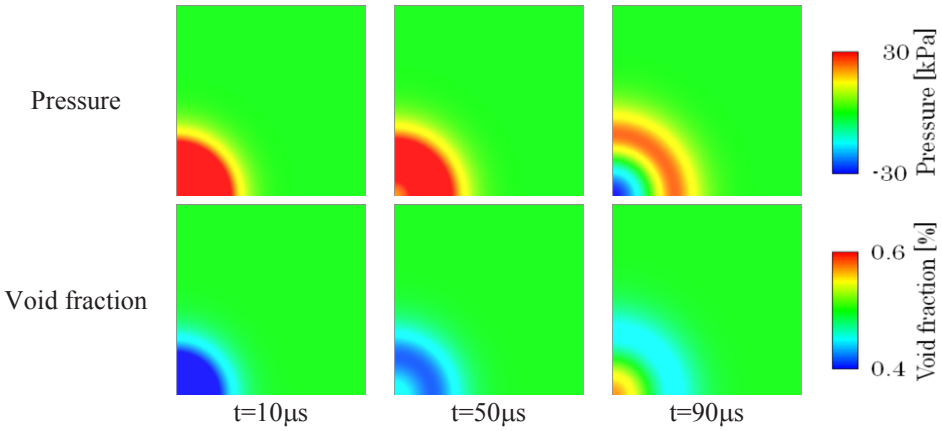

(a) Rigid wall

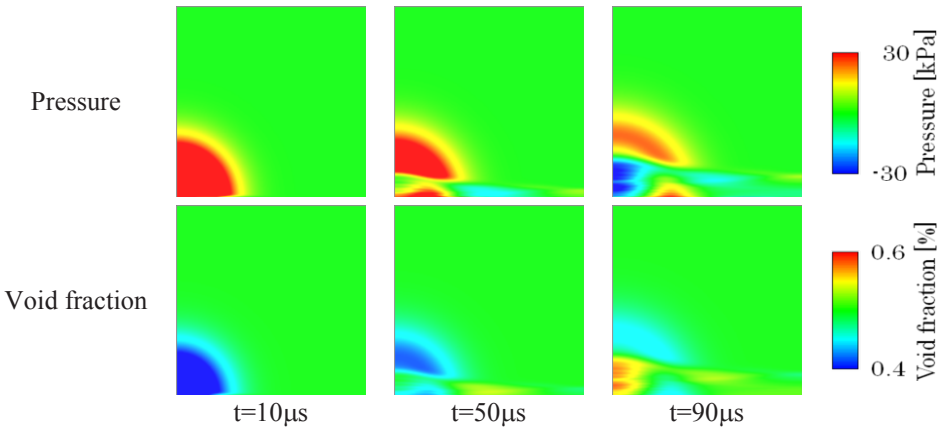

(b) Elastic wall

Figure 6: Time evolution of the pressure and void fraction distribution for f_{G0}=0.5%.

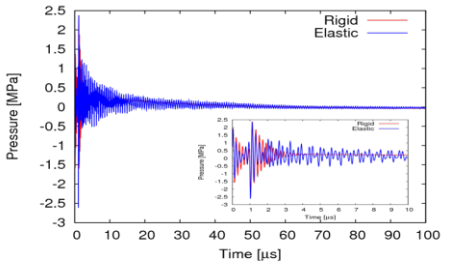

(a) Pressure at z=0mm

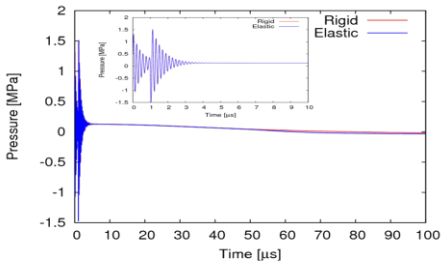

(b) Pressure at z=4.5mm

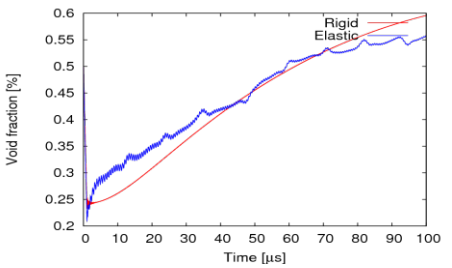

(c) Void fraction at z=0mm

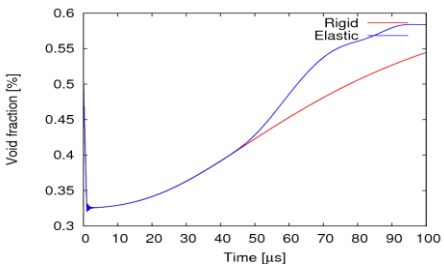

(d) Void fraction at z=4.5mm

Figure 7: Profiles of the pressure and void fraction at points of z=0, 4.5mm for f_{G0}=0.5%.